ICAS-88-4.2.1

COMPARISON OF DIFFERENTIAL REYNOLDS STRESS AND k-ε TURBULENCE MODELS FOR THE DRIVEN CAVITY PROBLEM

R.K. Cooper,
Queen's University of Belfast, Northern Ireland.

M. Wolfshtein,
Technion, Haifa, Israel.

M. Behnia, G. de Vahl Davis and J. Reizes,
University of New South Wales, Sydney, Australia.

Abstract

The differential Reynolds Stress transport model for turbulent flow is applied to the problem of recirculating flow in a rectangular cavity, driven by a moving wall. The model of Naot, Shavit and Wolfshtein is used to close the Reynolds stress equations. A dissipation equation is solved to provide a length scale, although an algebraic length scale model is also considered.

The predictions for the RS-ε model and the two equation k-ε model are compared with the experimental results of Normandin for a cavity of aspect ratio 3. There is a wall-jet like flow of high turbulent energy downstream of the moving wall, with strong diffusion of Reynolds stress from the jet towards the wall. The wall layer is thin, so is not resolved adequately by the uniform grid scheme. Conventional wall functions are found to be inadequate in this case, so we propose empirical "cavity jet boundary conditions", based on wall-jet and cavity jet data.

The predictions of the mean velocity field are fair, for both k-ε and RS-ε models. The turbulent energy and shear stress are low in the cavity jet region, but the distribution in the Reynolds stress model is closer to reality. The stabilising effect of flow curvature is captured by the RS model.

1. Introduction

Turbulent, recirculating flow in an enclosed cavity or box is a model for many flows of practical interest; ventilation or heating of a room, flow in a double glazing unit, wind driven flow in a reservoir, scavenging flow in an internal combustion engine, for example. Flow in a rectangular cavity, driven by a moving wall, exhibits many of the features of these applications, and is a useful test case for turbulence models.

The two equation k-ε, turbulent kinetic energy-dissipation model, has been used extensively for prediction of turbulent flows. The Differential Reynolds Stress transport model is neglected by comparison with the k-ε model, even though it is a better representation of the physics. Rodi (1) and Leschziner (2) have reviewed the turbulence models, including applications. This paper compares these models for a turbulent re-circulating flow in a rectangular cavity, driven by a moving wall, assuming the mean velocity field to be two dimensional.

Normandin (3) has obtained LDA measurements of the turbulent flow in a wall driven cavity of aspect ratio A = 3. (A is the ratio of "depth" to moving wall "length".) The flow consists of a main rotating cell or vortex, roughly centred in the cavity, with small cells in the lower corners, remote from the moving wall. Grand found the flow to be very sensitive to boundary conditions for aspect ratios greater than 3. We concentrate on the aspect ratio 3 cavity, relying on the experiment of Normandin for verification.

The Reynolds Stress model, with wall proximity corrections, has been successfully applied to flows in channels, ducts (straight and curved), wall jets and swirling flows, as described by Leschziner (2). In these cases the turbulence structure is evolving relatively slowly in the flow direction. Conversely, the separating and reattaching shear layer on a backward facing step is far from equilibrium, and is not well predicted by second order closure models, as shown by Amano and Goel (4). Similarly, regions of the driven cavity flow appear to be far from equilibrium, especially near the moving wall and in the wall-jet like flow downstream of the moving wall. Normandin drew an analogy between the "cavity jet" and the two-dimensional wall jet on a flat plate, and showed that the mean velocity profiles are similar. However, on comparing the turbulence properties, using data given in the review of Launder and Rodi (5), we find that the turbulent stresses in the cavity jet are 3 to 5 times larger than in the wall jet. The "wall functions" for the layer between the wall and the local velocity maximum are strongly affected by diffusion of stress from the jet region. Thus one of the main simplifying features of the numerical model is compromised. The solution would appear to lie with a fine grid resolution of the wall layer. We propose an alternative empirical solution: a cavity jet model, incorporating data from wall jet experiments, modified to give closer agreement with the limited cavity jet data.

2. Differential Reynolds Stress Model

Transport equations for the Reynolds stresses (second order correlations) contain

unknown terms which have been modelled by Naot, Shavit and Wolfshtein (6,7), and Launder, Reece and Rodi (8), amongst others. These models are similar, but that of Naot et al is used in this work. In addition to the equations for conservation of mass, momentum and the Reynolds stresses, a length scale or dissipation equation is required. In certain problems, such as duct flow, it is possible to specify the length scale algebraically.

The Reynolds stress transport equations pose particular problems, since they are stiff, due to the dominance of the algebraic production, redistribution and dissipation terms, over the differential convection and diffusion terms. Numerical instability is also a problem due to the coupling between the equations. Reitman et al (9) computed developing flow in a rectangular duct, by exploiting the nearly parabolic nature of duct flow, in which the influence of the downstream boundary condition is weak. The present study is in support of work on turbulent natural convection, Behnia et al (10), and is based on the code of Reitman et al, modified for two-dimensional flow in a rectangular region.

2.1 Governing Equations

The Reynolds averaged Navier-Stokes equations for incompressible flow are

$$\frac{\partial U_m}{\partial x_m} = 0$$

$$\frac{\partial U_i}{\partial t} + U_m \frac{\partial U_i}{\partial x_m} = -\rho^{-1} \frac{\partial P}{\partial x_i} + \nu \frac{\partial^2 U_i}{\partial x_m \partial x_m} - \frac{\partial \overline{u_m u_i}}{\partial x_m}$$

where U_i, P, $\overline{u_i u_j}$ are the mean velocity, mean pressure and the Reynolds stress tensor, respectively.

The transport equations for the Reynolds stresses are:

$$\frac{\partial \overline{u_i u_j}}{\partial t} + U_m \frac{\partial \overline{u_i u_j}}{\partial x_m} = V_{ij} + P_{ij} + T_{ij} + \Pi_{ij} - L_{ij}$$

The terms on the right are as follows.

Viscous transport, which is usually negligible compared to the turbulent transport;

$$V_{ij} = \nu \frac{\partial^2 \overline{u_i u_j}}{\partial x_m \partial x_m}$$

Production of Reynolds stress by the mean flow gradients;

$$P_{ij} = -\overline{u_i u_m} \frac{\partial U_j}{\partial x_m} - \overline{u_j u_m} \frac{\partial U_i}{\partial x_m}$$

Turbulent transport;

$$T_{ij} = -\frac{\partial \overline{u_m u_i u_j}}{\partial x_m}$$

Total pressure interactions;

$$\Pi_{ij} = -\rho^{-1} \left(\overline{u_i \frac{\partial p}{\partial x_j} + u_j \frac{\partial p}{\partial x_i}} \right)$$

Dissipation of Reynolds stresses by viscous action;

$$L_{ij} = 2\nu \overline{\frac{\partial u_i}{\partial x_m} \frac{\partial u_j}{\partial x_m}}$$

2.2 Modelling

The terms representing turbulent transport, pressure interaction and dissipation must be modelled to close the equations, and we follow Naot et al (7), with slight modifications to emphasise the similarity to other models.

For high Reynolds number flows, most of the dissipation occurs in small, locally isotropic eddys, thus

$$L_{ij} = \tfrac{2}{3} \delta_{ij} \epsilon .$$

Any non-isotropic dissipation is included in the "return to isotropy" term below. The dissipation of turbulent energy may be obtained from a transport equation, or in some cases, e.g. duct flows, may be obtained from an algebraic turbulence length scale l as follows;

$$\epsilon = C_D k^{3/2} / l$$

where the turbulent kinetic energy is

$$k = \tfrac{1}{2} \overline{u_i u_i} .$$

The turbulent diffusion is represented by a gradient diffusion model

$$T_{ij} = \frac{\partial}{\partial x_m} \left(\Gamma \frac{\partial \overline{u_i u_j}}{\partial x_m} \right)$$

where the diffusivity is specified by the Prandtl-Kolmogorov eddy viscosity

$$\Gamma = \nu_t = C_\mu \frac{k^2}{\epsilon} = C_\mu' k^{1/2} l .$$

The pressure interaction is modelled in two parts, representing: (1) the "return to isotropy" of anisotropic turbulence and (2) the forced interaction due to distortion of turbulence by the mean strain. For the first Rotta proposed

$$\Pi_{ij,1} = -A \frac{\epsilon}{k} \left(\overline{u_i u_j} - \tfrac{2}{3} k \delta_{ij} \right) .$$

Naot et al augmented this by a term of the same form as the γ term in the next equation, so we assume it to be included below.

The forced interaction or "rapid" term is modelled by

$$\Pi_{ij,2} = -\alpha \left(P_{ij} - \tfrac{1}{3} P_{ll} \delta_{ij} \right) + \beta \left(D_{ij} - \tfrac{1}{3} D_{ll} \delta_{ij} \right) + \gamma \tfrac{4}{3} k E_{ij}$$

where

$$D_{ij} = -\overline{u_i u_m}\frac{\partial U_m}{\partial x_j} - \overline{u_j u_m}\frac{\partial U_m}{\partial x_i}$$

$$E_{ij} = \frac{1}{2}\left(\frac{\partial U_i}{\partial x_j} + \frac{\partial U_j}{\partial x_i}\right).$$

The Reynolds stress model is completed by a transport equation for the dissipation, following the standard k-ε model in Rodi (1).

$$\frac{\partial \epsilon}{\partial t} + U_i\frac{\partial \epsilon}{\partial x_i} = \frac{\partial}{\partial x_i}\left(\frac{\nu_t}{\sigma_\epsilon}\frac{\partial \epsilon}{\partial x_i}\right) + \frac{\epsilon}{k}\left(C_{1\epsilon}P - C_{2\epsilon}\epsilon\right)$$

where the production of turbulent energy is

$$P = -\overline{u_i u_j}\frac{\partial U_i}{\partial x_j}.$$

Alternatively, the length scale may be specified algebraically, in which case we assume the same form as used by Naot et al (7) for the rectangular duct. For a cavity with sides a, b, and with n the normal distance from the nearest wall:

$$l_{max} = 0.135\min(a,b)$$
$$l = n \qquad n < l_{max}$$
$$l = l_{max} \qquad n \geq l_{max}.$$

The effect of a wall on the turbulence is to reduce the fluctuations normal to the wall and enhance the other direct stresses. Following Naot et al, we model this effect only on the "return to isotropy" term, by expressing Λ as a function of the length scale and near wall distance;

$$\Lambda = \Lambda_1 - (\Lambda_1 - \Lambda_2)l/n$$

where subscripts 1 and 2 indicate values away from wall effect and close to the wall, respectively. In applying this formula we have assumed the algebraic length scale above, even if the dissipation transport is evaluated.

2.3 Boundary Conditions

In the present study no attempt is made to compute the inner part of the turbulent boundary layer, since this would involve a much finer grid than is reasonable with the available code. Consequently we use the concept of wall functions, to model the constant stress (logarithmic) part of the turbulent boundary layer, and place the near wall grid point in this flow region. This procedure works well for duct and channel flows, since relatively thick, near equilibrium wall layers are established. However for the driven cavity flow, the wall layers are very thin, and so a fine grid would be required to encompass all the flow features, especially in the wall jet like region downstream of the moving wall. Notwithstanding this observation, conventional wall functions have been used, with modified boundary conditions for the cavity jet region.

The mean velocity profile near the wall is assumed to be a power law, modified by a mean shear term from the interior of the flow. This modification reflects the diffusion of shear stress towards the walls, thus reducing the mean velocity gradient. The modified power law specifies the near-wall tangential velocity in terms of two interior values. Numerically, the effect is to reduce the wiggles which appear on the velocity profiles. Central differencing is used throughout, with a staggered grid for the velocities, and this scheme is prone to wiggles of wavelength twice the grid interval. The normal velocity boundary condition is determined to conserve mass in the layer between the wall and the first (offset) velocity grid point.

The transport equations for the one dimensional equilibrium wall layer give solutions for the Reynolds stresses, with u in the flow direction and v normal to the wall:

$$\overline{u^2}/k = \tfrac{2}{3}(1 + (2 - 2\alpha - \beta)/\Lambda)$$
$$\overline{v^2}/k = \tfrac{2}{3}(1 - (1 - \alpha - 2\beta)/\Lambda)$$
$$\overline{w^2}/k = \tfrac{2}{3}(1 - (1 - \alpha + \beta)/\Lambda)$$
$$\overline{uv}/k = -v^{*2}/k = -A$$

where

$$A = \frac{1}{\Lambda}\sqrt{\frac{2}{3}(2\alpha + 4\beta - 2\alpha\beta - \alpha^2 - \beta^2 - 1 + \Lambda(1 - \alpha + \beta - \gamma))}$$

The friction velocity v^* is determined from the equilibrium wall layer, assuming a 1/7th power law to the first grid point.

$$\frac{U_1}{v^*} = 8.5\left(Re x_1 v^*\right)^{1/7}$$

Alternatively, the friction velocity may be determined iteratively from the logarithmic law of the wall. The flow prediction was found to be virtually the same for both methods.

The values of the parameters depend on the solutions of various equilibrium flows, and on empirical data. For the equilibrium wall layer (1)

$$C_\mu = A^2$$
$$C_D = A^{3/2}/\chi$$

where we take the von Karman constant to be

$$\chi = 0.4$$

It is usual to assume a compromise value

$$A = 0.3$$

whereas Naot et al suggest 0.2, a value which is low even for the wall layer. The full set of parameters is shown in Table 1.

Table 1. Parameters for RS-ε model

Λ_1	Λ_2		
1.6	0.6		
α	β	γ	
0.7558	-0.0465	-0.0619	
C_D	C_μ'	C_μ	χ
0.41	0.22	0.09	0.40
$C_{1\varepsilon}$	$C_{2\varepsilon}$	σ_ε	
1.44	1.92	1.30	
$A=\lvert\overline{uv}\rvert/k$	$\overline{u^2}/k$	$\overline{v^2}/k$	$\overline{w^2}/k$
0.30	1.26	0.29	0.45

u parallel to wall
v normal to wall

3. Numerical Method

It is convenient to use a non-dimensional system based on the moving wall length and velocity, and the density; henceforth all terms are non-dimensional. The momentum equations, continuity and the Reynolds stress transport equations are expressed in terms of the velocity components in the x and y directions, and the pressure, respectively

$$U, V, P$$

and the Reynolds stresses grouped as follows,

$$k = \tfrac{1}{2}\left(\overline{u^2} + \overline{v^2} + \overline{w^2}\right)$$
$$e = \overline{u^2} + \overline{v^2}$$
$$d = \overline{v^2} - \overline{u^2}$$
$$\overline{uv}.$$

The parabolic transport equations are solved by a finite difference procedure, using second order accurate central differencing. Uniform grid spacing is used in each direction over the rectangular computational domain. With a staggered grid for the velocities, mass and momentum are conserved. The momentum equations are solved for one time step, and the mass source error in each cell is evaluated. Following Briley (12), a potential velocity field sufficient to anihilate this mass source is added to give a corrected velocity field. The pressure field is found as the solution of a Poisson equation. The transport equations for the turbulent stresses and the dissipation (if required) are then progressed one time step.

The transport equations have the form:

$$\frac{\partial f}{\partial t} = -U\frac{\partial f}{\partial x} - V\frac{\partial f}{\partial y} + \frac{1}{Re}\left(\frac{\partial^2 f}{\partial x^2} + \frac{\partial^2 f}{\partial y^2}\right) + S.$$

The source term includes pressure gradient and Reynolds stress terms. The finite difference equivalent of the space operators may be written

$$Lf = (A_x + A_y)f.$$

The Alternating Direction Implicit method of Samarskii and Andreev (13) is used to march the solution forward in time. From the second order accurate time difference

$$\omega = \frac{f^{i+1} - f^i}{\Delta t} = \tfrac{1}{2}(A_x + A_y)(f^{i+1} + f^i) + S^i$$

the ADI splitting gives

$$(I - \tfrac{1}{2}\Delta t A_x)\omega^* = (A_x + A_y)f^i + S^i$$
$$(I - \tfrac{1}{2}\Delta t A_y)\omega^{**} = \omega^*$$
$$f^{i+1} = f^i + \Delta t\,\omega^{**}.$$

The Reynolds stress equations are stiff and strongly coupled due to algebraic terms. To alleviate this probem Reitman et al (9) used a three level splitting of the ADI scheme for the developing duct flow. However, the conventional two level splitting with source term (as above) was also found to be satisfactory for the driven cavity prediction.

For one time step, the numerical method involves application of the ADI procedure for each transport equation and solution of Poisson equations for the correction potential and pressure., If ADI is used to solve the Poisson equations iteratively, then this dominates the computational effort, taking about 90% of the time. We have used a direct method due to Christiansen and Hockney (14), based on the FFT and cyclic reduction. Each Poisson solution then takes about the same time as an ADI step. The procedure is also more robust, so larger time steps may be taken while avoiding instability. This code is at least ten times more efficient than the original version.

Incorporation of the transport equation for the dissipation causes stability problems. The time step required for the RS-ε method is 10% of that for the RS.a.l. method. Also, the time step for the turbulent stress and

dissipation equations is half that for the momentum equations, thus producing a false transient solution.

4. Turbulent Flow in a Rectangular Cavity

The experimental data of Normandin (3) for a cavity of aspect ratio 3, at a Reynolds number of 200,000, is the most complete set available for the driven cavity. The system of axes is defined in Fig. 1, with the origin at the bottom of the cavity, and moving wall at the top parallel to the y-axis. Distances and velocities are normalised on the moving wall length b, and velocity Vw, respectively. Normandin used axes with origin at the downstream end of the moving wall, and we indicate this system by an over-bar.

The moving wall creates a region of high shear stress which drives a jet like flow of high turbulent kinetic energy along the wall downstream of the moving wall. The cavity jet drives the main vortex as it runs down the wall, turns at the bottom of the cavity and returns up to the moving wall, to be partly entrained by the moving wall shear layer. The main vortex structure is shown in Fig. 2, by the stream function, normalised with respect to the moving wall length and velocity. The subsiduary vortices in the lower corners could not be resolved accurately due to three dimensional flow. Profiles of the velocity and Reynolds stresses at several stations on lines parallel to the moving wall are used for detailed comparison.

Initial computations with conventional wall functions and the Reynolds stress - algebraic length scale model (RS.a.1.) showed a three cell flow structure with the main vortex in the top one-third of the cavity, and lower cells of alternate rotation. It appeared that the wall layer was not energetic enough to remain attached to the downstream wall. After many numerical experiments, several strategies emerged which produced qualitatively correct flow structures, although not usually including the minor lower corner vortices. The strong diffusion from the vortex towards the walls was simulated by increasing the diffusion parameter C_μ' by a factor of 3 or 4. Alternatively, a local increase in C_μ' near the downstream wall was more effective, Fig. 4, thus emphasising the importance of this region. An increase in the "return to isotropy" parameter Λ, was also beneficial. It was somewhat disheartening to observe that the single equation kinetic energy - algebraic length model (k.a.1.) gave a physically realistic prediction, Fig. 3! Obviously a closer study of the experimental data was required.

4.1 Cavity jet boundary conditions

The computation of the driven cavity flow is strongly influenced by the boundary conditions on the downstream wall. The near wall flow structure is influenced by diffusion from the jet region, and thus the boundary layer type wall functions are of doubtful validity, at least for the relatively large grid intervals used.

The cavity jet is compared with the wall jet in stagnant surroundings, using a concensus of data from Launder and Rodi (5). The mean velocity profile is similar, as shown in Fig. 5(a). However the Reynolds stresses, k, $\overrightarrow{u^2}$ (u parallel to the wall) and $\overline{uv}$, normalised by the local maximum velocity, are substantially larger for the cavity jet; Figs. 5 (b),(c),(d). In the lower third of the cavity (away from the moving wall) the wall jet comparison breaks down, due to the adverse pressure gradient and flow curvature. The Reynolds shear stress is negative at the wall, but increases to a similar positive value at the position of the maximum velocity, and then increases further before decaying in the outer jet region. This is caused by strong diffusion due to the much larger length scale in the jet region than in the near wall region. The standard wall functions do not model these effects and no attempt has been made to derive wall-jet functions. However empirical functions are used to simulate turbulent stress boundary conditions which are a compromise between wall jet and cavity jet data.

The near wall behaviour of the cavity jet is modelled by the following approximations; for the point where the velocity is half of the maximum;

$$\bar{y}_{1/2} = 0.05 + 0.1\,\bar{x}$$

turbulent kinetic energy;

$$k/U_m^2 = 0.05 + 0.04\bar{y}/\bar{y}_{1/2}$$

and shear stress;

$$\overline{uv}/U_m^2 = -0.004 + 0.04\bar{y}/\bar{y}_{1/2}\ .$$

These formulae are applied to determine the boundary conditions for 80% of the downstream wall, assuming that the maximum velocity is approximated by the value at the near wall grid point. Conventional wall functions are applied for the remainder of the cavity.

4.2 Results and Discussion

The above boundary conditions have been applied to the k-ε and RS-ε models using the parameters in Table 1. The results for stream function are shown in Figs. 6, 7. Profiles along lines parallel to the moving wall of mean velocity, turbulent kinetic energy, and Reynolds stress are shown in Figs. 9 and 10. for stations x = 2.2 and x = 1.6 respectively.

The maximum value of the stream function is 0.025 at x = 1.6, y = 0.6, from the experiment of Normandin. The k-ε model overestimates the strength by about 5% and places the vortex centre well above mid-cavity at (2.0, 0.55) approximately. The RS-ε model slightly underestimates the strength, with centre at (1.6, 0.55). This good agreement may be fortuitous, since the results are sensitive to changes in certain parameters as discussed below.

It is clear that the wall jet boundary conditions have improved the prediction, confirming that the finite difference grid is too coarse, especially near the moving wall and downstream wall. The code could not be easily changed to accommodate a non-uniform grid, so this was not tested. Fig. 10 shows results obtained by Huang (16) (see also Leschziner (2)), with a RS-ε model, using third-order accurate quadratic upwind differencing (QUICK) for the mean velocity convection terms and a non-uniform grid. The mean velocity profiles are similar, but Huang overestimates the magnitude of the cavity jet.

The turbulent kinetic energy, Figs. 9(b), 10(b), is underestimated in the cavity jet region, even with the revised boundary conditions. The results of Huang show large gradients of k near the wall, in a region unresolved by our computation. Similar observations apply to the Reynolds shear stress $\overline{uv}$. Our predicted ratio of $\overline{uv}/k$ is close to 0.3 over most of the cavity, whereas the experimental value is significantly lower except in the jet region. The RS-ε model predicts the reduction in turbulent energy and shear stress in mid-cavity, due to the stabilising effect of flow curvature, as discussed by Leschziner (2).

The length scale extracted from the turbulent energy and dissipation

$$l = C_D k^{3/2}/\epsilon$$

is shown in Fig. 8 for the RS-ε model. The length scale increases with distance from the wall to more than twice the prescribed algebraic length scale. The lower length scale in the jet region apparently contradicts the explanation given above for the diffusion of Reynolds stress towards the wall. However there is a local maximum in the experimental value of the integral length scale in the jet region, and this is reflected by our empirical cavity jet boundary conditions. This is another feature which must be resolved by a finer computational grid. It is possible to alter the algebraic length scale to simulate this behaviour, but it detracts from the utility of the RS.a.l. model.

The anisotropy of the turbulence has been evaluated by comparing the ratios

$$\overline{u^2}/k, \quad \overline{v^2}/k, \quad \overline{w^2}/k.$$

The predicted values are approximately 1.0, 0.5, 0.5 over most of the cavity, where the velocity vector is approximately parallel to the side walls. However the experimental results of Normandin show the turbulence to be more isotropic (except in the lower one-third of the cavity), implying a stronger "return to isotropy" effect than accommodated by the model. This lends support to the suggestion of Gibson and Younis (14) for a simplified model with parameters;

$$A = 3.0, \quad \alpha = 0.3, \quad \beta = \gamma = 0.$$

Results obtained with this model show an increase in k, in accord with experiment, but more work is required.

Normandin obtained much larger values of turbulent energy in the lower half of the cavity than predicted. This may be due to the effect of flow separation and amplification of turbulence in the curved shear layers. Amano and Goel (4) have developed a third-order closure model and found it superior to second-order closures in predicting the high turbulence levels in the reattaching shear layer from a backward facing step. Similar features of the driven cavity flow are not captured by the second-order closure model, so the third-order model should be tried.

It should be noted that the turbulent diffusion model (triple correlation term) used in the present model, and also by Shir (15), differs from that of Launder et al (8). The method used to model the effect of wall proximity on the "return to isotropy" term also differs. The magnitude of the wall correction has a significant effect on the mean velocities and also interacts with the boundary conditions. These points are under investigation.

The present method is strongly influenced by the boundary conditions, and is sensitive to the distance from the wall to the near-wall grid point, at which boundary conditions are applied. For the results presented the (normalised) wall-to-grid distances are, for bottom wall, moving wall and side walls respectively;

$$x_{01} = 0.095 \qquad x_{02} = 0.025$$

$$y_{01} = 0.025 \qquad y_{02} = 0.025 \ .$$

The corresponding grid spacings for the 65 x 33 grid are

$$h_x = 0.045 \qquad h_y = 0.02969.$$

The corresponding value of the wall variable y+ (= y u^*/ν) is approximately 240 on the moving wall, and in the range 20-70 for the other walls, except near the corners. Reducing the wall-to-grid distances by 20% gave about 5% reduction in the mean velocity, and this is an undesirable feature of the numerical method. We conclude that a grid spacing sufficiently fine to resolve the near-wall structure of the flow is required. It appears that a low Reynolds number turbulence model, such as proposed by Adams and Rodi (17), may then be necessary to define the near-wall flow.

5. Conclusions

The predictions of the mean velocity field and turbulent stresses in the driven cavity are fair, for the second-order closure Reynolds stress - dissipation, RS-ε model, although revised values of some parameters are required. The Reynolds stresses in the wall-jet like flow downstream of the moving wall are much higher than in an equilibrium boundary layer, due to strong diffusion from the jet towards the wall. The correct cavity jet boundary conditions are approximated by an empirical model. This method

depends on assumptions of the extent and growth of the wall jet region, so may not be applicable to other geometries. The real solution is to resolve all significant flow structure in the wall layer, by using a sufficiently fine grid.

The k-ε turbulence model with the revised cavity jet boundary conditions is inferior to the RS-ε model for both mean flow and turbulence properties.

The algebraic length scale model must be revised to account for the effects of the cavity jet flow. This detracts from the utility of the RS.a.l. model, but the substantially increased stability and rate of convergence may be a factor in some applications.

Following Gibson and Younis (14) more weight may be given to the "return to isotropy" term, with a compensating reduction in the "rapid" term, in the pressure-strain correlation model. Computations have been done with this model, but there is unsufficient evidence to prefer it to the "standard" model.

The important cavity jet flow is not well predicted by the present Reynolds stress model. Amano and Goel (4) have developed a third-order closure model and found it superior to second-order closures for the reattaching shear layer. We have not yet compared these models, but the possibility of improvement remains.

Finally, much more program development and testing is required for an RS-ε model than for a k-ε model, and the latter gives roughly correct predictions of many complex flows. However for swirling flows the Reynolds stress model is superior.

6. Acknowledgments

Part of this work was done with the support of a Visiting Fellowship at the University of New South Wales.

We are indebted to Dr. M.A. Leschziner for enlightening discussions and for providing the results of Refs. 16 and 17.

7. References

1. Rodi, W., Turbulence Models and their Application in Hydraulics. I.A.H.R., Delft, 1980.

2. Leschziner, M.A. Numerical implementation and performance of Reynolds-stress closures in finite-volume computations of recirculating and strongly swirling flows. von Karman Institute for Fluid Dynamics, Lecture Series 1987-06, Introduction to the Modelling of Turbulence, 1987.

3. Normandin, M., Etude Experimentale de l'ecoulement turbulent dans une cavite profonde. Doctoral Thesis, Institut Mechanique, University of Grenoble, 1978.

4. Amano, R.S. and Goel, P., Investigation of Third-order Closure Model of Turbulence for the Computation of Incompressible Flows in a Channel with a Backward-facing Step. Trans. ASME, J. Fluids Eng., Vol. 109, 1987, 424-428.

5. Launder, B.E. and Rodi, W., The turbulent wall jet. Progress in Aerospace Sciences, Vol. 19, ed. P.J. Finley, Pergamon, 1982.

6. Naot, D., Shavit, A. and Wolfshtein, M., Two-point Correlation Model and the Re-distribution of a Reynolds Stresses. Phys. Fluids, Vol. 16, 1973, 738-743.

7. Naot, D., Shavit, A. and Wolfshtein, M., Numerical Calculation of Reynolds Stresses in a Square Duct with Secondary Motion. Warme and Stoffubertragung, Vol. 7, 1974, 151-161.

8. Launder, B.E., Reece, G.J. and Rodi, W., Progress in the development of a Reynolds stress turbulence closure. J. Fluid Mech., Vol. 58, 1975, 537-566.

9. Reitman,V., Israeli,M. and Wolfshtein,M., Numerical Solution of the Reynolds Stress Equations in a Developing Duct Flow. AIAA Paper No. 83-1881, 1983.

10. Behnia, M., Cooper, R.K., de Vahl Davis,G., Leonardi, E., Naot, D., Reizes, J.A. and Wolfshtein,M. Turbulent Natural Convection in a Rectangular Cavity. Int. Symp. Comp. Fluid Dyn., CTAC-87, Sydney, 1987.

11. Briley, W.R. Numerical Method for Predicting Three-dimensional Steady Viscous Flows in Ducts, J. Comp. Phys., Vol.14, 1979, 8-28.

12. Samarskii, A.A. and Andreev, V.B., USSR Comp. Math. & Math. Phys. Vol. 3, 1963, 1373-1382.

13. Christiansen, J.P. and Hockney, R.W., DELSQPHI, a Two-dimensional Poisson-solver Program. Computer Phys. Comm. Vol. 2, 1971, 139-155.

14. Gibson, M.M. and Younis, B.A., Calculation of swirling jets with a Reynolds stress closure. Phys. Fluids Vol. 29(1), 1986, 38-48.

15. Shir, C.C., A Preliminary Numerical Study of Atmospheric Turbulent Flows in the Idealized Planetry Boundary Layer. J. Atmos. Sci., Vol. 30, 1973, 1327-1339.

16. Huang, P.G. The computation of elliptic turbulent flows with second-moment-closure models. Ph.D. Thesis, Univ. of Manchester, 1986.

17. Adams, E. and Rodi, W., Computer results for a lid driven cavity flow using low Reynolds number turbulence models. Univ. Karlsruhe, F.R. Germany.

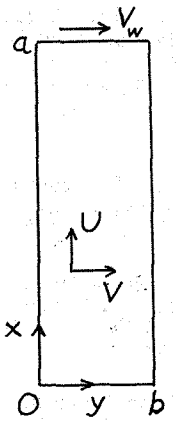

Fig. 1.
Driven cavity coordinate system.

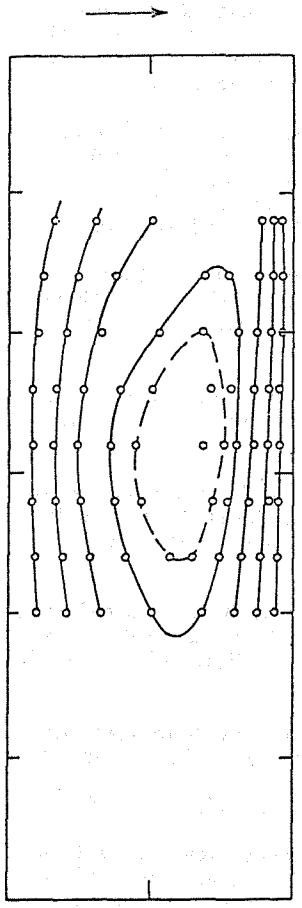

Fig. 2.
Normalised stream function
Experiment of Normandin.
A=3. Re=200000.
Contour interval —— 0.005
- - - 0.0025

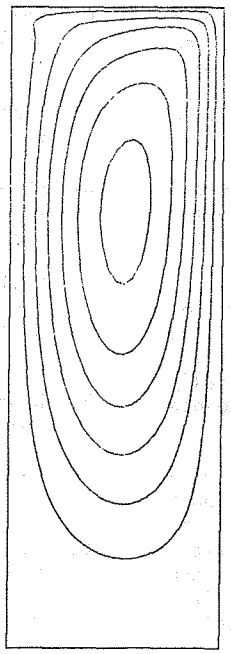

Fig. 3.
Normalised stream function
k.a.l. model.
A=3. Re=200000. 49x25 grid
Wall function b.c.
Contour interval 0.005

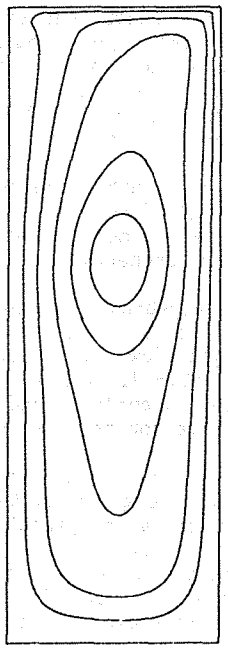

Fig. 4.
Normalised stream function
RS.a.l. model.
A=3. Re=200000. 65x33 grid
Wall function b.c.
Contour interval 0.005
$C_\mu' = 0.22\ (1+4y^4)$

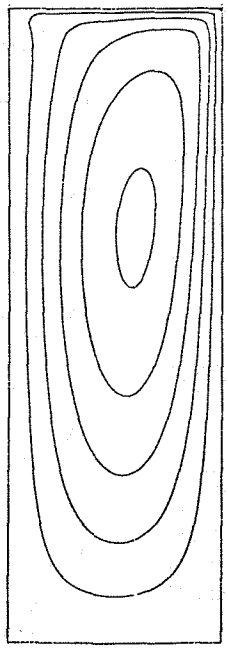

Fig. 6.
Normalised stream function
k-ε model.
A=3. Re=200000. 65x33 grid
Cavity jet and wall function b.c.
Contour interval 0.005

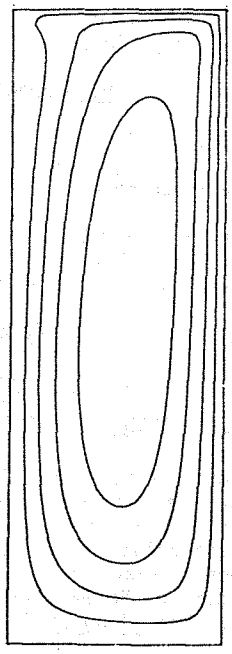

Fig. 7.
Normalised stream function
RS-ε model.
A=3. Re=200000. 65x33 grid
Cavity jet and wall function b.c.
Contour interval 0.005

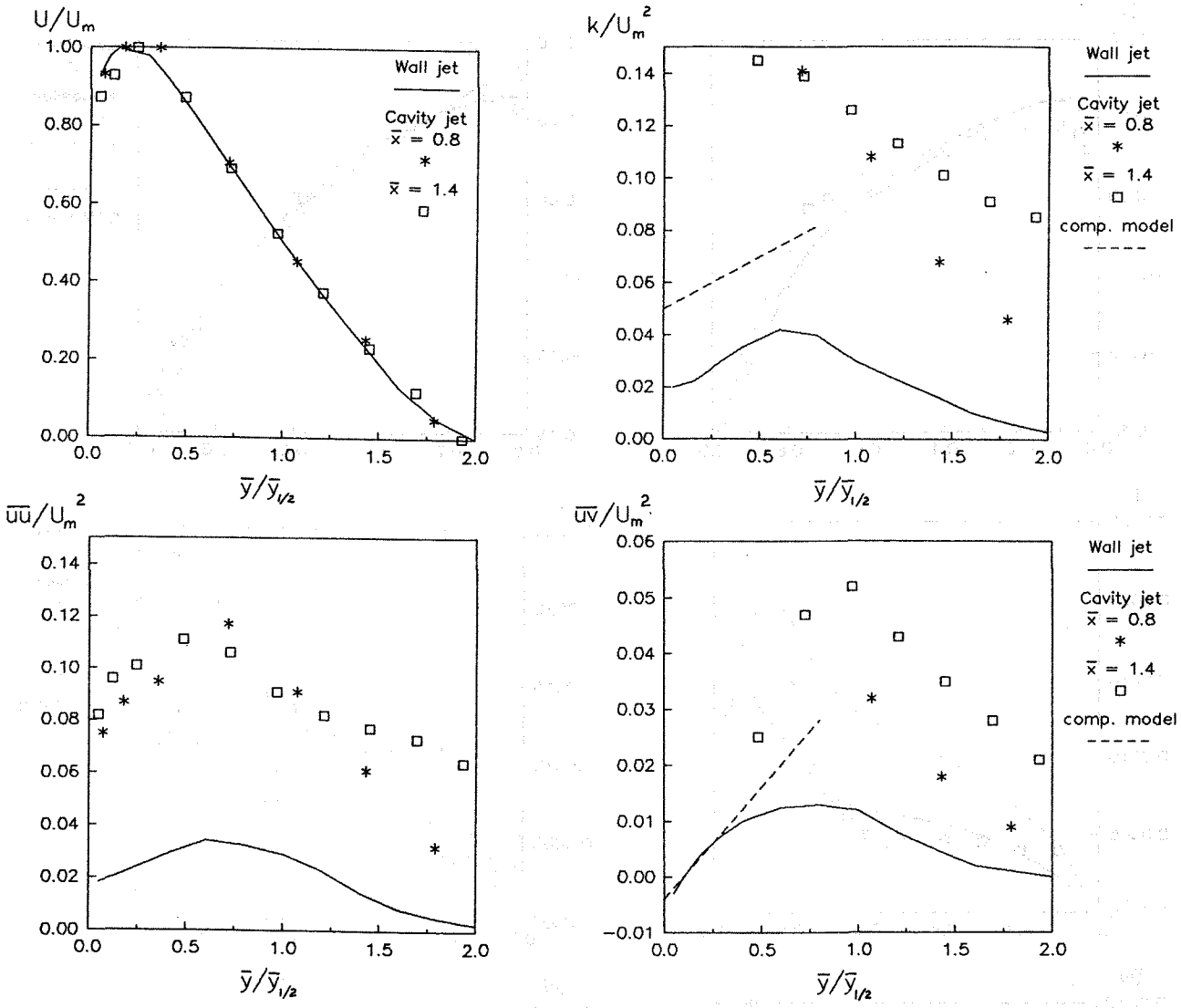

Fig. 5. Comparison of wall jet and cavity jet data, normalised with respect to local maximum mean velocity.
(a) Mean velocity U (b) Turbulent kinetic energy, k
(c) Reynolds stress, $\overline{uu}$ (d) Reynolds stress, $\overline{uv}$

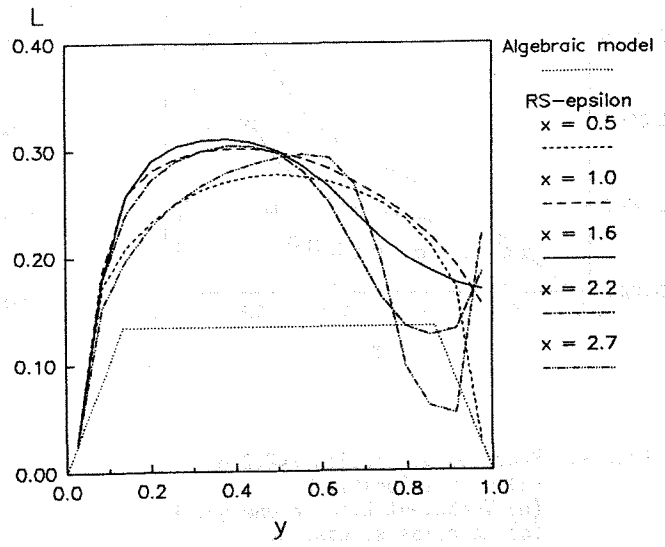

Fig. 8. Length scale from RS-ε model

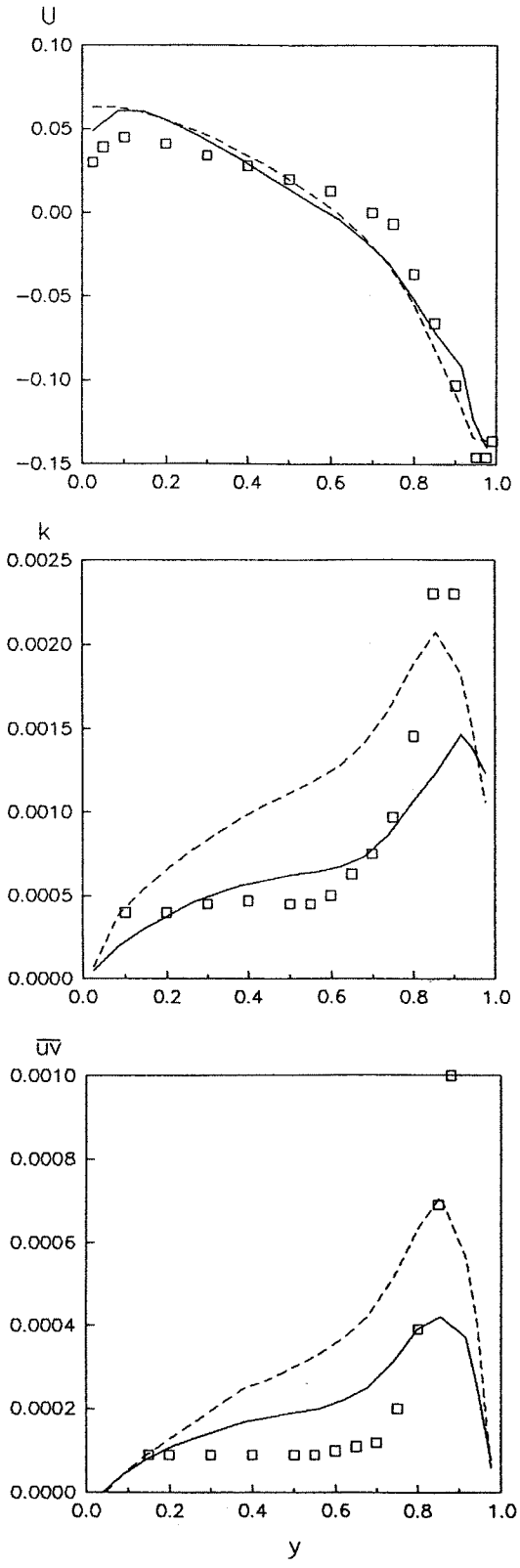

Fig. 9. Profiles at station x=2.2 of
(a) Mean velocity, U
(b) Turbulent kinetic energy, k
(c) Reynolds stress, $\overline{uv}$

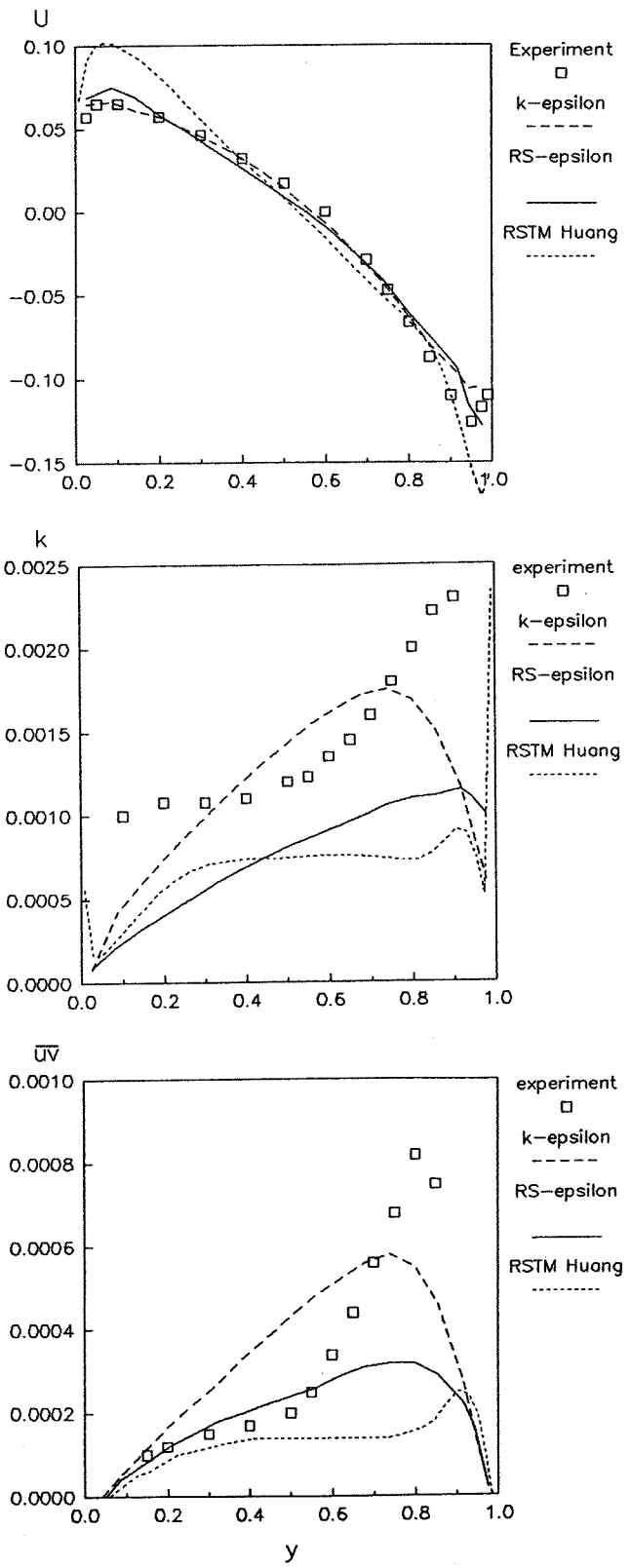

Fig. 10. Profiles at station x=1.6 of
(a) Mean velocity, U
(b) Turbulent kinetic energy, k
(c) Reynolds stress, $\overline{uv}$